

**Palaeo-redox conditions of groundwater during glaciation at Sellafield, UK revealed by
SIMS analysis of REE in fracture-fill calcite**

*England, G.L.¹, Gillespie, M.R.², Milodowski, A.E.³, Haszeldine, R.S.¹, Degnan, .P.J.⁴ and Bath
A.⁵*

¹ *School of GeoSciences, The University of Edinburgh, West Mains Road, Edinburgh, EH9 3JW,
UK (Corresponding Author e-mail: s.haszeldine@ed.ac.uk Fax (+44) (0) 131 668 3184)*

² *British Geological Survey, Edinburgh, EH9 3LA, UK*

³ *British Geological Survey, Keyworth, Nottingham, NG12 5GG, UK*

⁴ *United Kingdom Nirex Limited, Curie Avenue, Harwell, Didcot
Oxfordshire OX11 0RH, UK*

⁵ *Intellisci, Willoughby on the Wolds, Loughborough LE12 6SZ*

10 May RSH

Abstract

Reconstruction of palaeo groundwater redox chemistry is essential to enable a forecast of future groundwater conditions. This is particularly important at sites proposed for nuclear waste repositories, which will experience glaciations within the future 10^6 years. A record of ancient palaeo-water is held in the growth layering of calcite crystals which have formed during the last 2 Ma. Modern oxidised groundwaters frequently show Ce depletion anomalies in REE profiles. In this study at Sellafield (UK), we use detailed SIMS analyses examine the REE-geochemistry of geologically young fracture-fill calcite as an indicator of palaeo-redox conditions. At Sellafield, the shallowest fracture-fill calcites, show Ce depletion anomalies (by a factor of 100) within crystal growth zone micro-stratigraphy. These record shifts of +120mV in Eh. Ce depletion also coincides with independent evidence: 1) Calcites at shallow depth have low Mn and Fe contents, with fluctuating Mn:Fe ratios between 0.1 and 100 (oxidised); contrasting with deeper high Mn and Fe contents and a Mn:Fe ratios of 2 (reduced). 2) Shallow Fe-Mn (hydr)oxides co-precipitated with calcites to 450m, but (reduced) sulphides gradually become associated with calcites from 850m depth. 3) Calcite crystals change from nailhead to dogtooth shapes at 325-360m, because of a transition from freshwater to saline water (15g/l chloride). 4) Deep redox is calculated to be -100 to -240mV from equilibrium with pyrite. We interpret that Ce depletion shows that very oxidised palaeo-waters have certainly invaded sporadically to at least 236m. These were probably sub-glacial. Brackish palaeo-waters to 450m are more reduced, and deep saline palaeo-waters to 1527m are the most reduced. We demonstrate that the fine resolution afforded by SIMS analysis permits the detailed unravelling of 10-50 micron micro-stratigraphy held in zoned mineral cements. This is believed to be the first study of palaeo-groundwater in the UK at this level of spatial resolution.

Keywords:

Radioactive waste, repository performance, hydrogeology, geochemistry, cerium, oxidation

Disposal of radioactive waste deep below ground requires a detailed understanding of past and future states of groundwater hydrogeology, in order to predict rates and pathways of flowing groundwater leachate that may be contaminated with radionuclides. Geochemical understanding of individual sites is necessary, as the particular chemistry of groundwater and rock mass can significantly affect radionuclide transport properties. In particular, changes in redox conditions can be important, for example reducing conditions, negative Eh, provides a useful geochemical constraint on the mobility of aqueous uranium complexes. Consequently, to enable a predictive assessment of performance at an individual disposal site, information is required to reconstruct past groundwater origins, chemistries and redox. Swedish measurements of groundwater geochemistry in crystalline rocks using hydrogen and oxygen isotopes (Wikberg, 1993, Laaksoharju et al., 1999) have shown that glacially derived water may infiltrate to 500-600 m. Bath et al (2005a) show with salinities, stable isotopes and noble gases that that meteoric derived freshwater recharged to 350-700 m at Sellafield UK. Zuber et al. (2004) has also demonstrated isotopically that glacially derived waters occur in deep sedimentary aquifers in Poland. However, evidence based on depleted $\delta^{18}\text{O}$ in groundwater does not necessarily indicate the redox conditions which existed at the time of infiltration, since oxygen that was dissolved in such water could have been consumed by reductive buffering by the host rocks, especially by reactive Fe^{II} minerals.. Rivas-Perez et al. (2003) explain that oxidative fronts in fractures advance very slowly, some 4000 times slower than groundwater flow rates. Consequently, additional evidence of ancient oxidation is needed to indicate whether large palaeo-fluxes of O_2 (aq) have occurred.

One method of capturing such information is to seek natural geochemical tracers held in diagenetic minerals that precipitated from ambient groundwater in the host formation during glacial water infiltration. In understanding redox change, we need to examine elements that appear to respond to such changes. In studies of groundwater, negative Ce anomalies in Rare

Earth Element (REE) profiles (normalised to chondrite) are frequently considered to relate to the decrease in solubility that accompanies the oxidation of Ce^{3+} to Ce^{4+} . Therefore Ce depletion has been used to support interpretations of oxidizing conditions (e.g. Brookins, 1989; Braun et al., 1990; Dia et al., 2000; Yan et al., 2001).

Figure 1 here

One common mineral that has been recognised as useful in providing information is calcite (Vaniman and Chipera, 1996; Denniston et al., 1997; Wallin and Peterman, 1999; Bath et al., *in preparation*). Calcite typically exhibits zoning on a tens of micron scale, which should record changes in local groundwater. This micro-stratigraphy is readily observable by cathodoluminescence, and sometimes contains fluid inclusions, which hold micro-samples of an ancient porewater. Yet, in many cases, the fine-scaled nature of the mineral zoning present in calcites (i.e. < 50 microns) and the low concentrations of many trace elements (< 50 ppm) mean that it is difficult to measure the detailed record visible from microscopic stratigraphy. In this study, we geochemically examine finely-zoned cathodoluminescent calcites by high-resolution sampling (< 20 microns) using ion microprobe (SIMS) analysis. The calcites in this study form volumetrically minor linings to fractures hosted in Ordovician meta-volcanic, to Triassic sedimentary, rocks cored from boreholes located in the Sellafield area, on the Cumbria coast of NW England (Fig. 1). Until 1997, the site was extensively investigated by United Kingdom Nirex Limited as a potential location for a deep repository for the disposal of intermediate to low-level radioactive waste (Bowden et al., 1998; Gillespie and Milodowski, 2003; Degnan et al., 2003). We demonstrate that REE geochemistry of fracture-fill calcite can preserve detailed information about the depth of penetration of oxidised waters into the subsurface within the past few thousand years.

Geological and Hydrological Settings

The calcite we have examined comes from the surfaces of open fractures in two adjacent boreholes (PRZ2 and BH2) drilled in the “Proposed Repository Zone” (PRZ) at Sellafield (Fig. 1). The boreholes penetrate strata up to ~1500 m deep below sea level (b.o.d.). From base to surface, these comprise the: Borrowdale Volcanic Group (Ordovician); Brockram conglomerates of the Appleby Group (Permian); the Sherwood Sandstone Group (Triassic), and unlithified Quaternary clay, sands and gravels. Further to the west, additional boreholes intersected the same stratigraphy, with the inclusion of Dinantian age Carboniferous Limestone, and St Bees Shale and Evaporites of the Cumbrian Coast Group (Permian). There are at least nine episodes of fracture mineralization in the area, previously identified by Milodowski et al. (1998). The most recent mineralization events (ME8 and ME9), are dominated by Mn oxy-hydroxides and euhedral calcite respectively. These are considered to have a relationship to Quaternary and present-day groundwater conditions. This study has analysed calcites by ion microprobe, to produce unusually precise data on REE profiles at high resolution. This is believed to be the first study of palaeo-groundwater in the UK at this level of resolution.

Figure 2 here

Hydrogeologically at the present day, three distinct groundwater domains have been identified in the Sellafield area (Black and Brightman, 1996, McKeown et al., 1999). These include: 1) the “Coastal Plain Regime” that consists of rapidly-flowing topographically-driven meteoric water; 2) the “Hills and Basement Regime” consisting of saline waters up to 30 g/l TDS, with slow groundwater flow; and 3) the “Irish Sea Basin Regime” consisting of halite derived brines, predominantly west of the current coastline and essentially stagnant. Using the most recent calcite crystals which line the fractures, an association was identified by Milodowski et al., (1997), between crystal morphology and present-day groundwater salinity; this is observed in many of the site investigation boreholes (Fig. 2). The crystals demonstrate: c-axis shortened

forms (referred to as “nailhead”) in the fresh groundwater zone; changing to more equant forms as salinity increases in the ‘morphological transition zone’ (MTZ), observed in boreholes near the present zone of mixing between fresh groundwater and saline basement water; to finally c-axis elongate crystals (referred to as “dogtooth”) that occur in the more saline basement water.

The calcites also demonstrate differences in cathodoluminescence (CL), with the youngest calcite growth zones above the MTZ being predominantly non-luminescent (with only minor fine yellow growth bands). In contrast below the MTZ, the calcites demonstrate finely banded yellow, orange and red luminescent zones (Milodowski et al., 1997). Luminescence in calcites is predominantly controlled by variation in Mn^{2+} that activates luminescence, and Fe^{2+} that quenches luminescence (Marshall, 1988). Changes in luminescence can therefore represent changes in redox-potential, and therefore provide an indication of Eh redox conditions in past groundwaters, from which the calcites precipitated (Machel and Burton, 1991). As well as this change in luminescence, co-precipitating mineral phases at Sellafield also suggest a difference in redox conditions with depth. Marcasite and pyrite (sulphides) are associated with calcites in the deeper parts of the profile (~ below 850m), and are suggestive of reducing conditions. By contrast, nearer to the surface, Fe and Mn oxyhydroxides have precipitated, indicative of more oxidising conditions (Haszeldine et al., 1996, Milodowski et al., 1998). Present-day groundwater regimes at Sellafield are considered to represent a slowly-adjusting dynamic equilibrium between the pressures of elevated onshore topographically-driven fresh water, sea water at the coast, and dense brine that occurs at depth in offshore formations. However during glacial and especially de-glacial groundwater conditions, these equilibrium conditions readjust - initially because of the topographic head of water in the ice sheet, and later due to the upwelling of groundwater into eskers (Boulton et al., 1993). Sub-glacial water is typically highly oxygenated, due to the air bubbles entrapped in ice, raising the possibility that deep penetration of very oxidising groundwater could occur. This could have adverse consequences for the waste

retention performance of a repository if the oxygenated water were to penetrate to repository depth (Boulton and Curle, 1997).

The youngest fracture-filling calcites in the MTZ record changes of crystal morphology (relating to salinity) and depict a complex CL zonation pattern. Milodowski et al. (1997, 1998) which suggests that the MTZ (which can be at least 300m vertically) may represent a zone where the groundwater regimes have shifted from fresh “meteoric” to saline “basement” conditions (and vice-versa) over time. The present-day groundwater change from “fresh” to “saline” occurs over a Saline Transition Zone (STZ) of only a few tens metres. Thus, the detailed zonation and chemistry of these calcites may hold a record of changes in ancient groundwater – the challenge is to access and interpret that record. To further examine this important geochemical attribute within the profile, calcite samples were methodically selected from core at different depths in two closely spaced boreholes adjacent to Borehole 2. Four samples were selected as representing typical fracture-filling calcite morphologies present within the vertical profile at the Sellafield site (Fig. 2) and are described in Table 1. Two of these samples are at the present-day zone of salinity change. The largest crystals (1.0 to 0.5 mm) from within these samples were selected for analysis to maximise the number of analyses that could be performed. Extensive petrographic investigations were made before REE analyses, so that the CL growth zonation of crystals analysed in detail is known to be typical of samples across the Sellafield Site.

Methodology

Minor and trace (REE) element analysis were performed by SIMS, on individual CL zones to produce a profile across an individual crystal. Analyses were carried out using the CAMECA IMS 4f instrument located at Edinburgh University, UK. Techniques and data corrections applied are similar to those developed by Dawson and Hinton, (2003). The elements analysed included Ca, Mn, Fe, Mg, Sr, Na, Y, Li, Ba, La, Ce, Nd, Sm, Eu, Dy, Er and Yb (although only

Fe, Mn and REE are reported in this paper). The analytical conditions during two sessions were 10 nA $^{16}\text{O}^-$ measurements of positive secondary ions, with a 120 eV energy offset. Ten cycles were performed (over ~ 25 minutes per analysis) with the first two cycles eliminated, to reduce the possibility of surface contamination. Analyses were also corrected for background. The ion microprobe spot diameter was 10 to 20 microns, enabling analyses to be performed within individual CL zones in most cases, and at a spacing closer than 50 microns if required. The laboratory standard used was the Oka calcite and statistical counting errors varied, but generally were < 1% for concentrations above 100 ppm, while for concentrations below 10 ppm errors were 10-15%.

Rare Earth Element analyses from the surrounding host rocks were made by Milodowski (unpub) using standard ICP techniques. This enables comparison of fracture-fill calcite REE profiles with host-rock REE profiles.

General Results: Mn, Fe ; REE

Full results of the ion microprobe analyses of calcites from Sellafield are listed in Table 2. Given that this paper is concerned with elements that may provide an insight into redox conditions, we will concentrate only on manganese, iron and the rare earth elements.

Figure 3 here

Figure 4 here

Manganese and Iron

Ion-microprobe analyses of calcites from Sellafield demonstrate an overall increase in concentration of both Fe and Mn with depth (Fig. 3). This co-variant pattern is suggestive of either: a decrease in calcite precipitation rate at deeper burial; an increase in water/rock interaction; or an increase in temperature (Myers, 1991). As also observed in previous studies of

calcite at Sellafield (Milodowski et al., 1997; Milodowski et al., 1998), Fe and Mn abundances appear to fluctuate according to the degree of luminescence of individual zones. At Sellafield, the range of this fluctuation appears to generally decrease with depth, which may also be indicative of increasing geochemical stability of groundwaters with greater depth, particularly in relation to perturbation of redox conditions by water influx (Milodowski et al., 1998). For example, the deepest sample from 1527m (Fig. 4, and 5d) demonstrates only slight changes in Mn to Fe ratios (~ 2 to 3), with only subtle variation in orange CL. By contrast, the youngest zones of calcite in the shallowest sample at 236m (Fig 4 and 5a) (that occurs within the current freshwater regime), have extreme variation of Mn to Fe ratios (~ 0.1 to 100), displaying significant CL changes from yellow to dark orange and poorly luminescent burgundy luminescent zones. These same outermost (youngest) growth zones in sample 236m also have dull CL illumination, with minor brighter zones. Our petrographic studies of other samples shows that this is typical of samples in the fresh water regime (Milodowski et al., 1998), enabling us to use the 236 m sample as a ‘representative’ crystal.

Figure 5 here

REE elements

Unlike Mn and Fe concentrations, Σ REE (total REE concentration) in calcite does not greatly vary with depth. The main change is that the innermost part of samples at 1527m and 413 m have lower Σ REE than the outer zones. Individual crystal samples vary internally in Σ REE from 1-2 ppm to 350 ppm. In some cases, Σ REE fluctuates according to luminescent zonation, in other cases, the cause for changes in Σ REE is less apparent. When ion-microprobe REE data of calcite is chondrite-normalised (according to Anders and Grevasse, 1989), most profiles display a flat or slight hump-like pattern, associated with Medium (M) REE enrichment, compared to Light (L) REE or Heavy (H) REE. (Fig. 5a to 5d). Slight fluctuations in the chondrite-normalised profiles are evident internally within each zoned crystals, as well as between sample depths.

Partitioning behaviour between REE in natural aqueous solutions and precipitating calcite is poorly understood (Zhong and Mucci, 1995). Consequently it is not clear whether the overall chondrite-normalised profiles we observe in a calcite at Sellafield are the same as that of the solution it precipitated from. However, the variation in chondrite-normalised patterns are most likely influenced by fluctuations in: 1) groundwater Eh-pH-salinity conditions; 2) complexes by which the REE are carried within the groundwater; 3) and the source of the REE elements themselves, considered to be influences from the host rock. At this Sellafield site, geochemical analyses of REE from the BVG host bedrock at Sellafield reveal no negative Ce anomalies (Fig. 6), and neither do REE analyses from the host St Bees Sandstone (Fig 7), consequently a host-rock control in this setting is improbable. REE profiles from different calcites at Sellafield show shallow samples with Ce depletion, and deep samples without Ce depletion (Fig 5). Consequently, these effects are believed to result from changes in redox, which can be considered on Eh-pH cross-plots.

REE results from each sample

In the deepest sample (1527m, Fig. 5d) within dogtooth crystals, the core displays a low-abundance, irregular chondrite-distribution of REE. As the crystal zones become younger, LREE and MREE become more enriched, but HREE concentrations remain relatively low. A negative Eu anomaly is evident in the outer rim zones; this is strongest at the core / rim contact, and becomes weaker as the crystal becomes younger. The calcite at this depth is hosted within the Borrowdale Volcanic Group (BVG), which also displays a negative Eu anomaly (Fig. 6, Table 3) with a depletion of HREE, similar to the outer calcite zones. It is possible therefore that the Eu anomaly is a reflection of the local host rock influence, its signal becoming weaker as calcites begin to coat the fracture walls and allowing less water interaction with the host BVG. Similarly at the nuclear waste repository site at Yucca Mountain, Nevada, negative Eu anomalies

are evident in both host volcanics and fracture fill calcites (Vaniman and Chipera, 1996; Denniston et al., 1997). Although Eu is sometimes used as an indicator of redox conditions, these changes between Eu^{2+} and Eu^{3+} are generally restricted to higher temperatures associated with igneous and hydrothermal activity (Henderson and Pankhurst, 1984). At temperatures and redox conditions that are typical of normal groundwater systems, Eu^{3+} is the stable oxidation state. It is reduced to Eu^{2+} only in conditions more reducing than -0.35 volts and over the pH range of about 6 to 9 (Fig. 7).

At 413 meters depth, the next deepest calcite crystal sampled (Fig. 5c) is also hosted within the BVG, and is below the present-day groundwater STZ. This crystal also exhibits a zonation with a profile $\text{LREE} > \text{MREE}$, and slight HREE depletion similar to the BVG host rock. The youngest CL zones display slight MREE enrichment compared to LREE and HREE. All profiles demonstrate a slight positive Eu anomaly. Although the reason for this is speculative, one possibility is that this anomaly reflects local feldspar dissolution from the upper portions of BVG. The breakdown of feldspars can be the source of Eu enrichment in groundwater (Yan et al. 2001).

At 310 meters depth (Fig. 5b) the sample is situated in Brockram sandstone host rock just above the groundwater STZ at 325m, and calcite has equant crystals. A pronounced humped profile of MREE enrichment is evident, particularly in the central portion of the crystal. Eu is part of this positive enrichment, rather than individually enriched. The zoned rim surrounding the central portion demonstrates several luminescent zones with a similar pattern, while other zones demonstrate irregular profiles, with generally depleted REE.

At 236m, the shallowest sample is located within the current fresh water zone (Fig. 5a), and the calcite has an equant / nailhead form. The central parts of the crystal display bright CL, and

show a uniform profile with MREE enrichment, similar to the outer zones of 310m. Eu is relatively slightly more enriched, and La and Yb are variable relative to chondrite. The dark CL zones in the outer part of the crystal display a MREE profile enriched relative to chondrite, similar to that seen in the outer zones of deeper crystals. A prominent difference is the presence of a strong negative Ce anomaly relative to LREE in all analyses from the youngest (dark CL) growth zones, this is about 10 x depleted. Eu is relatively enriched in only two of these analyses.

In summary, a strong Ce depletion, relative to LREE, exists in the outer zones of the shallowest crystal, with Ce depletion absent in all deeper samples to 1527m. Eu enrichment, relative to MREE, occurs in all samples, but at 1527m Eu is enriched relative to MREE. The whole REE profile is similar to, but not identical to, the BVG in samples from 413m and 1527m, which are hosted by BVG.

Figure 6 here

Figure 7 here

Previous applications of depleted Ce anomaly as redox indicator

Most authors consider that REEs from saline near-surface acid, neutral, or alkaline waters exist as dicarbonate $\text{Ln}(\text{CO}_3)_2$ complexes, particularly for HREE, and are effectively scavenged from solution by Fe+Mn-oxyhydroxide phases which precipitate as the pH of the system rises towards neutral. Thus the dominant (>90%) control on REE abundance in near surface water is pH, although DOC, SO_4 , Fe and Al contribute significantly. Moller et al (1993) first observed Ce enrichment in modern aerobic alkaline waters, due to Ce^{3+} oxidation to Ce^{4+} with decreased pentacarbonate complex solubility. Following this, Leybourne et al (2000) and Yan et al (2001) proposed that in the weathered zone, rapid oxidation of Ce^{3+} to Ce^{4+} occurs, with preferential removal of Ce^{4+} from solution upon leaving the shallowest groundwater environment. This depletes Ce concentration of waters, which can be carried to near-surface unweathered sediment

– and so produces a negative Ce anomaly in precipitated minerals affected by aerobic water zones.

In the Carnmenellis area of SW England, the REE content of shallow groundwater derived from metasediments and granite is controlled by pH, with higher levels in groundwaters of pH < 6. Only REE in waters derived from metasediments display negative Ce and Eu anomalies, thought by Smedley (1991) to reflect Ce and Eu depletions present in the host meta-sedimentary bedrock. Alternatively, we suggest that the negative Ce anomaly in the Carnmenellis groundwaters may reflect the consequences of aerobic surface waters migrating into deeper host rock, given that isotopic evidence (Pyrillos et al 1998) suggests a meteoric influence throughout the weathering history. Modern groundwaters derived from Sardinian Hercynian granodiorites also show depletion of Ce (Biddau et al 2002), even though surface waters (presumably more aerobic?) show no such anomaly. Shallow groundwaters in NE Canada metasediments analysed by Leybourne et al (2000) show anomalies of Ce depletion. Again in this case, deeper groundwaters have no Ce anomaly and are characterised by REE patterns that are similar to the host lithologies.

Denniston et al. (1997) studied REE in fracture-fill calcites from Yucca mountain. They suggest the presence or absence of a negative Ce anomaly in calcite may be: 1) related to local REE source; 2) related to the effects of co- or pre- precipitating phases; or 3) associated with the *pH/Eh* conditions of the groundwater. Ce depleted anomalies are observed within both luminescent and non-luminescent zones of fracture-fill calcites in the “Upper Unsaturated Zone” (UUZ) at Yucca Mountain (Vaniman and Chipera, 1996; Denniston et al., 1997). However, deeper (~1000 m subsurface) calcite samples in the saturated level at Yucca Mountain do not contain any Ce anomaly. The interpretation for this observation is that Ce⁴⁺ present within oxidised groundwater is being preferentially scavenged by pre- and co-precipitating manganese oxide phases present in

the fractures in the UUZ, leaving depleted Ce concentrations to form calcite. By contrast, deeper saturated samples that have higher water to rock interaction dilute the effects of such Ce-scavenging (Vaniman and Chipera, 1996; Denniston et al., 1997), and may be dominated by the local composition of the rock, with more Ce.

Figure 8 here

Figure 9 here

Discussion of present and palaeo-redox

At the Sellafield site, we interpret the presence or absence of a negative Ce anomaly to be a reflection of groundwater *Eh*, rather than the influence of Ce-scavenging by other phases. The position with depth of the Ce anomaly determined in our work, appears to fit with previous interpretations of redox boundaries within the Sellafield subsurface (Haszeldine, et al., 1996, Milodowski et al., 1997, Milodowski, 1998, Bath et al., *in press*).

The analyses of Eu and Ce in zoned calcites can be used to constrain palaeo-Eh. In the site under investigation, we know that groundwater today (Nirex 1998) has measured of 6.2 to 7.8, and that Ce above the STZ is $< 0.3\mu\text{g/l}$ (2×10^{-9} Molar), and groundwater below the STZ has Ce $< 15 - 20 \mu\text{g/l}$ (1.8×10^{-7} Molar). Both Eu and Ce can exist in two oxidation states. For Eu, this is dependent on Eh, but for Ce there is a co-dependence on pH and on Eh. Firstly examining Eu (Fig. 8), we can see from the analysed REE profiles (Fig. 5) that there is minimal Eu variation. From this we can infer that Eh remained more oxidising than -360mV, and Eu concentration is not sensitive to that. Secondly for Ce (Fig.9), we can see that profiles from the shallower samples (Fig. 5) are depleted in Ce by a factor of 100 in some calcite zones. Assuming that the pH range of present day waters is similar to that of palaeo-waters, then this Ce variation can be most simply explained by a variation in Eh. We illustrate this by using a mid-range present-day

pH of 7.0, and the present-day measured water concentrations of Ce (Fig.8). A paleo-Eh variation of 120 mV would produce a Ce redox change from Ce^{3+} to Ce^{4+} , and so enable the aqueous solubility change by a factor of 100, which results in Ce depletion by a factor of 100 within the calcite crystal zone. This would occur if Eh varied between +40 and +160mV, at a pH of 7.0. In the most alkaline pH measured (7.8), the same 120mV shift, from -150 to -30mV, would produce a similar Ce solubility change by a factor of 100. The process is therefore independent of the exact pH. The fact that Ce depletion of palaeo-water is only recorded in the uppermost sample, and occurs there in only discrete zones, suggests that Ce solubility was not subject to small fluctuations in Eh. This means that that groundwater Eh did not normally lie on the Ce redox boundary, but was sufficiently reduced that redox fluctuations did not cross over into the field of Ce oxidation. We infer that palaeo-waters at 236m usually had Eh more reduced than +50mV, and could have been more reduced than -150mV.

Figure 10 here

At the Sellafield PRZ, a Ce depletion anomaly is only detected in the shallowest (236 m) sample, whereas Mn and Fe oxyhydroxides are present to depths of 300 metres (Fig. 10). These minerals are interpreted to have formed prior to, and during, the youngest non- luminescent calcite mineralisation, related to supergene alteration and weathering by near surface groundwaters. Coeval with this mineralisation, in deeper groundwater conditions, pyrite and marcasite precipitated in associations with luminescent calcite (Milodowski et al, 1998). In-situ measurement of Eh in the BVG below 300m shows Eh as +50 to + 90mV. However calculated Eh suggests that this could be substantially more reduced, with Eh being -100 to -240mV, based on equilibrium mineral assemblages including iron pyrites. Our results suggest that in a profile moving up the borehole, we begin to observe changes in palaeo-redox conditions just below where saline dogtooth calcite changes to C-axis flattened (nailhead) calcite, which starts to

appear in the Morphological Transition Zone (Fig. 2). Unlike the calcite at UUZ Yucca Mountain, only the non-luminescent calcite phase exhibits a Ce negative anomaly. Non-luminescent calcite that formed in the Freshwater Zone and upper MTZ at Sellafield is interpreted to have precipitated in paleo-oxidised conditions (Bath et al. 2005b in press). In the shallowest (236 m) calcite crystal examined (located within the current freshwater zone), the Ce anomaly begins to appear in the non-luminescent calcite near the outer edge of the dogtooth to equant crystal, and then has a stronger signature associated with younger nailhead overgrowth calcite when Mn decreases (Fig. 4a, 5a). We deduce that calcite morphology changes with salinity change at 325m in the MTZ (as suggested by Milodowski, et al, 1998). Paleo-redox conditions, as recorded by proxies such as Mn:Fe ratio, and abundance of Fe+Mn-oxy-hydroxides, become systematically less-reduced towards shallower depth, and especially shallower than 300m.

Figure 11 here

Paleo-redox conditions, as measured by CL colour, become more oxidised above 236m. Paleo-redox conditions, as measured by Ce depletion become oxidised (Eh more than +100mV) shallower than 236m. This change in conditions seems to record a shift in the boundary between oxidised and the “reduced + freshwater zone” downwards, very late in the paragenetic sequence. Such a downward shift may have resulted from deeper penetration of abnormally oxygenated water derived from wet-based glaciers within the past 5,000 – 20,000 yr (Fig. 11). As yet, we have no measured age-dates of resolution comparable to that of the CL calcite zones or the REE analyses.

With similar fracture-fill calcite evident in other localities in Europe (e.g. Åspo Sweden; Dounreay, Scotland), this micro-stratigraphy and REE micro-analysis technique could be

potentially employed in site-specific paleohydrogeological investigations for future nuclear waste depositories to test past redox changes.

Conclusions and Implications

1. Multiple SIMS analysis of REE from Quaternary dated, zoned, fracture-fill calcite crystals from 236 to 1527m subsurface at Sellafield (UK) reveal REE profiles which are predominantly enriched relative to chondrite-normalised profiles. The majority of profiles display relatively flat patterns with minor differences in some LREE and HREE fractionation, or humped patterns rich in MREE. The profiles from deeply buried crystals are similar to the host Borrowdale Volcanic Group meta-volcanics. Shallower depth REE profiles are more erratic. Variations in individual REE profiles may reflect changes in palaeo-hydrogeology, producing different mixes of water sources and ionic compositions. The inter-bedding of different profile 'fingerprints' within individual crystals forms a micro-stratigraphy of past water fluctuations.
2. Anomalies of Ce depletion by a factor of 100 are present in many of the outermost (youngest) calcite zones from shallow depth, 236m. Ce depletion is interpreted to result from oxidation of the palaeo-water by +120mV, which occurred during growth of the youngest calcite zones at 236m, and crossed the Ce^{3+} to Ce^{4+} boundary. However the outermost zones from deeper calcites show no Ce depletion. Such shifts of oxidised water towards at deeper 310m to 1527m either did not occur, or were masked by more reducing conditions.
3. Independent evidence of redox fluctuation at shallow depth is Mn:Fe ratios (0.1 – 1,000) with zoned CL from orange (oldest) to dark (youngest). Progressively more reducing conditions at greater depth are shown by constant ratios (Mn:Fe = 2) and uniform orange CL, with no dark zones deeper than 410m, and the sporadic occurrence of sulphides deeper than 850m. Mn-Fe (hydr)oxides occur as co-precipitated vein linings at depth

shallower than 300m, which we interpret to indicate weakly +ve Eh, whereas deeper than 850m more reducing waters (-ve Eh) permitted gradual precipitation of Fe-sulphides.

4. Fracture-fill calcites at shallow depth are flattened 'nail-head' habit, whereas calcites at deep depth are "dog-tooth" habit. The change in habit coincides with a present-day change from shallow fresh water, to saline water below 325m. Sectional profiles across calcite crystals at 236m show that the ancient change to nail-head habit, coincides with darker CL, and coincides with Ce depletion. At the present day, the Fe oxide to sulphide transition is deeper than the zone of salinity transition, which is deeper than the zone of Ce depletion. These are incremental measures of decreasing Eh away from the surface.
5. We suggest that deepest waters at Sellafield have remained reduced (Eh <0mV) during the Quaternary growth of these calcites. Any fluctuations of Eh deeper than 325m, are not well recorded by REE measurements. An episode of strongly oxidising paleo-water certainly penetrated down to at least 236m. This paleo-water would plausibly be sourced from the beneath a wet-bed glacier, with dissolved air bubbles within the ice contributing oxygen, and the topographic head of ice driving deeper water penetration.

Acknowledgements

This study was carried out as part of a EU Funded PADAMOT project (FIKW-CT-2001-00129). The authors would like to thank the staff (Richard Hinton, Nicola Cayzer, Simone Kasemann, John Craven) at the NERC funded Edinburgh University Materials and Micro-Analysis Centre for assistance with the ion microprobe and SEM.

References

- Anders, E., Grevasse, N. 1989. Abundances of the elements: meteoritic and solar. *Geochimica et Cosmochimica Acta*, 53, 197-214
- Bath, A., Richards, H., Metcalfe, R., McCartney, R., Degnan, P. and Littleboy, A. 2005a
Geochemical Indicators of Deep Groundwater Movements at Sellafield, UK. *Journal of Geochemical Exploration*. Spec Issue Geochemical aspects of radioactive waste disposal (Eds

- Peyaud, J.B., de Putter, T., McKinley, I.) in press
- Bath, A., Milodowski, A., Tullborg, E-L., Karki, A., Ruotsalainen, P., Shepherd, T., Cortes Ruiz, A., Aranyosy, J-F. 2005b. Palaeohydrogeological information from secondary calcite in fracture rocks at European sites. *Chemical geology*, in revision
- Biddau R., Cidu R., Frau F. 2002. Rare earth elements in waters from the albitite-bearing granodiorites of Central Sardinia, Italy. *Chemical Geology*, 182, 1-14.
- Black, J.H., Brightman, M.A., 1996. Conceptual model of paleohydrogeology of Sellafield. *Quarterly Journal of Engineering Geology*, 29, S83-S94.
- Boulton, G. S., Curle, F., (Eds), 1997. *Simulation of the effects of Long-Term Climate Change on Groundwater Flow and Safety of Geological Disposal 1997*. European Commission, Nuclear Science and Technology Series, Luxembourg, EUR 17793 En.
- Boulton, G.S., Slot T., Blessing, K., Glasbergen, P., Leijnse band, T, van Gijssel, K., 1993. Deep circulation of groundwater in overpressured subglacial aquifers and its geological consequences. *Quaternary Science Reviews*, 12, 739-745
- Bowden, R.A., Bumpus, C., Littleboy, A.K., 1998. An overview and update of the site characterisation studies at Sellafield. *Proceedings of the Yorkshire Geological Society*, 52, 125-137.
- Braun, J-J., Pagel, M., Muller, J-P., Bilong, P., Michard, A., Guillet, B., 1990. Cerium anomalies in lateritic profiles. *Geochimica et Cosmochimica Acta*, 54, 781-795.
- Brookins, D.G., 1989. Aqueous geochemistry of rare earth elements. In Lipin, B.R. & McKay, G.A. (Eds). *Geochemistry and Mineralogy of Rare Earth Elements*. Mineralogical Society of America Vol. 21, pp. 201-225.
- Dawson, J.B., Hinton, R.W., 2003. Trace-element content and partitioning in calcite, dolomite and apatite in carbonatite, Phalaborwa, South Africa. *Mineralogical Magazine*, 67, 921-930.
- Degnan, P.J., Littleboy, A.K., Michie, U.McL., Jackson, C.P. and Watson, S.P. 2003. Fracture-dominated flow in the Borrowdale Volcanic Group at Sellafield, NW England: the identification of potential flowing features, development of conceptual models and derivation of effective parameters. In: Petford, N. and McCaffrey, K.J.W. (Eds) *Hydrocarbons in Crystalline Rocks*. Geological Society of London Special Publication 214, 197 – 219.
- Denniston, R.F., Sheare, C.K., Layne, G.D., Vaniman, D.T., 1997. SIMS analysis of minor and trace element distributions in fracture calcite from Yucca Mountain, Nevada, USA. *Geochimica et Cosmochimica Acta*, 61, 1803-1818.
- Dia, A., Gruau, G., Olivie-Lauquet, Rio, C., Molenat, J., Curmi, P., 2000. The distribution of rare earth elements in groundwater: assessing the role of Source-rock composition, redox changes and colloidal particles. *Geochimica et Cosmochimica Acta*, 64, 4131-3151.

- Gillespie, M.R., and Milodowski, A.E., 2003 The palaeohydrogeological evolution of the deep groundwater system from Sellafield, recorded by late-stage fracture-lining calcite *Geochimica et Cosmochim Acta* 67, (18) A120-A120.
- Haszeldine R.S., 1996. Subsurface geology, geochemistry, and water flow at a Rock Characterisation Facility (RCF) at Longlands Farm: Supplementary. In: Haszeldine R S & Smythe DK (Eds), Radioactive waste disposal at Sellafield UK. University of Glasgow, pp 165-173.
- Henderson, P., Pankhurst, R.J., 1984. Rare Earth Element Geochemistry. Elsevier, New York, 467p.
- Laaksoharju M., Tullborg E.L., Wikberg P., Wallin, B., Smellie, J. 1999. Hydrogeochemical conditions and evolution at the Aspo HRL, Sweden. *Applied Geochemistry*, 14, 835-859.
- Leybourne, M.I., Goodfellow, W.D., Boyle, D.R., Hall, G.M. 2000. Rapid development of negative Ce anomalies in surface waters and contrasting REE patterns in groundwaters associated with Zn-Pb massive sulphide deposits. *Applied Geochemistry*, 15, 695-723.
- Machel, H.G., Burton, E.A. 1991. Factors governing cathodoluminescence in calcite and dolomite, and their implications for studies of carbonate diagenesis. In: Barker, C.E. and Kopp, O.C. (Eds), *Luminescence Microscopy: Quantitative and Qualitative Aspects*, SEPM (Society for Sedimentary Geology) Short Course 25, 37-57.
- Marshall, J.D., 1988. *Cathodoluminescence of Geological Materials*. Allen and Unwin Inc., Boston. 146p.
- McKeown, C., Haszeldine, R.S., Couples, G.D., 1999. Mathematical modelling of groundwater flow at Sellafield, UK. *Engineering Geology*, 52, 231-250.
- Milodowski, A.E., Gillespie, M.R., Metcalfe, R., 1997. Relationships between mineralogical transformations and groundwater chemistry at Sellafield, NW England: a tool for studying Quaternary palaeohydrogeology. In: Hendry, J.P., Carey, P.F., Parnell, J. Ruffell, A.H. & Worden, R.H. (Eds). *GEOFLUIDS II '97. Contributions to the Second International Conference on Fluid Evolution, Migration and Interaction in Sedimentary Basins and Orogenic Belts* (Belfast, 10-14 March 1997). University of Belfast, Belfast, 30-33.
- Milodowski, A.E., Gillespie, M.R., Naden, J., Fortey, N.J., Shepherd, T.J., Pearde, J.M., Metcalfe, R., 1998. The petrography and paragenesis of fracture mineralization in the Sellafield area, west Cumbria. *Proceedings of the Yorkshire Geological Society*, 52, 215-241.
- Moller, P., Bau, M. 1993 Rare-earth patterns with positive cerium anomaly in alkaline waters from Lake Van, Turkey. *Earth and Planetary Science Letters*, 117, 671-676.
- Myers, W.J., 1991. Calcite cement stratigraphy: an overview. In: Barker, C.E. and Kopp, O.C. (Eds), *Luminescence Microscopy: Quantitative and Qualitative Aspects*, SEPM (Society for Sedimentary Geology) Short Course 25, 133-149.
- Nirex, 1998. *Sellafield Geological and Hydrogeological Investigations. Compilation of*

- Reconnaissance Studies for Selected Isotope, Gas and Trace Element Data from Sellafield. Sellafield Geological and Hydrogeological Investigations. Science Report SA/97/090. UK Nirex Ltd, Harwell.
- Psyrillos, A., Manning, D.A.C., Burley, S.D. 1998. Geochemical constraints on kaolinization in the St Austell Granite, Cornwall, England. *Journal of the Geological Society*, 155, 829-840.
- Rivas-Perez, J, Tullborg, E.L., Banwart, S.A., 2003. The kinetics of O₂(aq) reduction during oxidative weathering of naturally occurring fracture minerals in groundwater *Mineralogical Magazine*, 67, 399-414.
- Smedley, P.L., 1991. The geochemistry of rare earth elements in groundwater from the Carnmenellis area, southwest England. *Geochimica et Cosmochimica Acta*, 55, 2767-2779.
- Vaniman D.T., Chipera, S.J., 1996. Paleotransport of Lanthanides and Strontium recorded in calcite compositions from tuffs at Yucca Mountain, Nevada, USA. *Geochimica et Cosmochimica Acta*, 60, 4417-4433.
- Wallin, B., Peterman, Z., 1999. Calcite fracture fillings as indicators of Paleohydrogeology at Laxemar at Åspö Hard Rock Laboratory, southern Sweden. *Applied Geochemistry*, 14, 953-962.
- Wikberg, P., Smellie, J., Wallin, B., Tullborg, E-L., Laaksoharju, M., 1993. Experiences from geohydrogeochemical investigations at the Åspö HRL site in Sweden. pp 219 -236 In: *Paleohydrogeological methods and their applications* OECD, Paris
- Yan, Xiu-Ping, Y, Kerrich, R., Hendry, M.J. 2001. Distribution of the rare earth elements in pore waters from a clay-rich aquitard sequence, Saskatchewan, Canada. *Chemical Geology*, 176, 151-172.
- Zhong, S., Mucci, A., 1995. Partitioning of rare earth elements (REEs) between calcite and seawater solutions at 25°C and 1 atm, and high dissolved REE concentrations. *Geochimica et Cosmochimica Acta*, 59, 443-453.
- Zuber, A., Weise, S.M., Motyka, J., Osenbrück, K., Rózanski, K. 2004. Age and flow pattern of groundwater in a Jurassic limestone aquifer and related Tertiary sands derived from combined isotope, noble gas and chemical data. *Journal of Hydrology*, 286, 87-112.

**Palaeo-redox conditions of groundwater during glaciation at Sellafield, UK revealed by
SIMS analysis of REE in fracture-fill calcite**

England, G.L.¹, Gillespie, M.R.², Milodowski, A.E.³, Haszeldine, R.S.¹, Degnan, .PJ.⁴ and Bath A.⁵

¹ *School of GeoSciences, The University of Edinburgh, West Mains Road, Edinburgh, EH9 3JW,
UK (Corresponding Author e-mail: s.haszeldine@ed.ac.uk Fax (+44) (0) 131 668 3184)*

² *British Geological Survey, Edinburgh, EH9 3LA, UK*

³ *British Geological Survey, Keyworth, Nottingham, NG12 5GG, UK*

⁴ *United Kingdom Nirex Limited, Curie Avenue, Harwell, Didcot
Oxfordshire OX11 0RH, UK*

⁵ *Intellisci, Willoughby on the Wolds, Loughborough LE12 6SZ*

DIAGRAMS

10 May RSH

Table 1.

Short descriptions of calcites analysed from fracture-lining in core at Sellafield UK. Depths are metres below Ordnance Datum (sea level).

Sample depth (BoD)	Position in current groundwater regime	Calcite morphology	CL characteristics
236m, Fig. 5a (borehole PRZ2)	Fresh water	Equant to dog tooth, with nail head overgrowth	Equant to dogtooth calcite consists of concentric zones of firstly intermediate-orange and yellow luminescent bands, followed by a younger poorly luminescent dark orange-burgundy zone and brightly luminescent yellow-orange outer band. The darker zones show evidence of dissolution / reprecipitation. The nail-head overgrowths also exhibit poorly luminescent dark orange-burgundy calcite.
310m, Fig. 5b (borehole PRZ2)	Fresh water, immediately above the Saline Transition Zone	Equant to dog tooth	A texturally disturbed (possibly dissolved and re-precipitated) red and orange core, followed by concentric growth zones of light-intermediate-dark yellow, orange.
413m, Fig. 5c (borehole PRZ2)	Saline Transition Zone	Dog tooth	A relict core of earlier mineralised calcite, followed by concentric growth zones of light-intermediate-dark yellow, orange and red luminescent bands.
1527m, Fig. 5d (borehole 2)	Saline Basement	Dog tooth	Two distinct zones: 1) outer rim, dark to intermediate orange luminescence, with faint micro-scaled concentric zonation; and 2) a slightly brighter, non-zoned core, with orange / yellow mottled patches reflecting possible dissolution – reprecipitation.

Table 2

Fe, Mn and REE results of SIMS analyses of calcite, data in ppm units. BDL = below detection limit. Code is for sample depth and analysis number, eg S326-1 is from 326 metres, analysis number 1.

s2362-	15	14	20	19	2	13	12	1	11	5	7	6	10	8	9	3	4	18	16	17
fe	115.8	25.4	494.7	1021.0	154.3	11.7	8.1	0.1	0.1	4.2	20.4	61.7	23.1	41.4	16.9	21.1	0.10	28.6	15.6	352.2
mn	2.3	6.1	32.7	26.4	2132.8	715.7	0.3	0.3	0.4	336.2	2080.0	4627.5	1481.9	754.7	1247.9	133.9	227.1	447.1	26.7	1049.3
la	6.70	2.63	3.52	2.95	1.80	0.07	0.26	BDL	0.08	1.31	1.77	2.47	0.21	0.98	0.50	11.77	0.68	3.19	1.18	4.36
ce	0.28	0.89	0.66	0.27	11.31	0.03	BDL	BDL	BDL	4.98	13.41	18.25	4.19	10.39	8.61	26.66	6.50	13.17	5.68	20.16
pr	2.73	2.39	3.88	2.34	2.23	0.25	0.18	0.26	0.13	1.14	2.19	2.76	0.69	1.75	1.14	3.21	1.29	1.90	1.63	2.75
nd	13.99	18.89	28.10	15.46	14.37	0.86	3.09	2.88	0.82	7.94	12.04	15.01	5.45	12.24	10.35	18.85	8.56	10.83	13.42	16.89
sm	4.23	6.75	11.54	5.70	6.77	1.36	0.50	2.68	BDL	3.19	5.80	5.37	3.50	6.83	5.55	5.50	4.22	4.82	6.21	7.10
eu	1.96	2.25	4.23	2.17	2.67	0.61	1.50	1.47	0.50	1.44	2.51	3.06	1.67	3.36	3.73	2.49	2.11	2.11	3.04	2.93
gd	8.11	6.21	10.92	8.02	9.49	1.91	3.26	4.48	1.60	5.31	6.31	7.80	5.13	10.56	7.14	8.39	5.40	5.55	8.72	6.42
gd	6.85	5.20	10.91	5.57	6.80	2.28	1.39	4.16	0.67	4.03	5.73	5.72	4.61	8.85	5.98	3.18	5.61	6.24	9.11	7.04
dy	3.56	3.54	7.13	3.06	5.72	3.07	2.73	4.98	2.78	3.42	3.16	4.65	3.47	7.05	5.44	4.09	2.85	3.82	5.21	4.66
er	1.12	1.27	1.72	1.41	2.30	0.42	2.04	1.53	0.12	0.61	1.09	0.73	0.44	2.50	1.46	1.84	0.66	1.04	0.94	1.42
yb	1.08	1.16	3.32	1.20	3.27	0.55	0.72	1.81	0.24	0.29	0.31	0.93	1.36	3.64	2.45	0.49	BDL	1.65	0.54	0.49
mn/fe	0.10	0.24	0.10	0.10	13.8	61.1	0.1	2.8	3.7	80.5	102.1	75.1	64.2	18.2	74.0	6.3	2271.2	15.6	1.7	3.0
REE (total)	50.6	51.2	85.9	48.1	66.7	11.5	15.8	24.4	7.1	33.7	54.3	66.7	30.7	68.1	52.3	86.5	38.0	54.3	55.7	74.2
la/sm	0.0	0.2	1.3	0.1	0.2	0.3	0.2	0.1	0.1	0.0	5.0	0.3	0.0	0.2	0.9	0.1	0.4	0.4	0.3	0.2
Gd/yb	1.9	1.7	5.4	463.7	11.6	5.1	15.1	2.0	2.0	2.8	2.3	1.6	3.4	3.7	5.3	13.8	11.9	3.1	3.8	2.7
la/yb	0.0	0.4	15.9	44.8	3.0	1.7	3.7	0.2	0.1	0.1	0.2	0.2	0.1	1.5	4.1	1.4	5.9	1.3	1.6	0.7

S310-	4	5	1	2	3	6	7	8	9	10	11	12
fe	1404.6	1275.0	3296.8	3186.8	3308.2	1347.0	1543.6	1496.4	1389.2	1838.7	1665.7	1608.5
mn	4159.8	4050.0	8013.8	7729.7	7956.8	6270.6	7169.2	7894.9	6690.8	6296.3	4514.2	6644.1
la	6.53	12.22	3.43	4.46	5.06	0.25	0.01	0.00	0.55	0.54	0.18	5.58
ce	32.98	49.39	17.81	23.00	26.18	1.86	0.12	0.21	1.46	2.95	1.20	26.44
pr	6.31	9.15	4.02	4.85	5.86	0.42	0.06	0.03	0.25	0.51	0.18	4.45
nd	42.17	52.87	28.70	33.98	40.63	3.97	0.26	0.40	1.10	4.55	1.06	22.93
sm	19.99	20.88	18.85	17.35	22.22	2.20	0.07	0.62	0.67	2.75	0.57	8.33
eu	6.61	7.65	6.90	6.95	8.93	0.61	0.11	0.22	0.28	1.07	0.40	2.84
gd	19.71	19.46	19.78	20.53	22.14	1.27	0.38	0.39	1.14	3.45	1.44	7.72
gd	20.15	20.80	20.61	19.00	24.15	1.45	0.60	0.47	0.95	3.20	0.76	6.76
dy	16.19	16.16	13.76	11.23	14.70	0.47	BDL	0.39	1.13	2.59	1.23	4.73
er	5.18	4.73	4.03	3.28	3.81	0.21	BDL	BDL	0.11	0.55	0.01	0.76
yb	0.02	BDL	BDL	BDL	BDL	BDL	0.13	BDL	BDL	BDL	BDL	BDL
mn/fe	3.0	3.2	2.4	2.4	2.4	4.7	4.6	5.3	4.8	3.4	2.7	4.1
ree(total)	175.8	213.3	137.9	144.6	173.7	12.7	1.7	2.7	7.6	22.2	7.0	90.5

s413	1	2	3	4	5	6	7	8	9	10	11	12	13	14	15	16	17	18	19	20	23	25	26	24	22	21
fe	4751.1	4233.4	2109.4	3833.0	3511.0	1502.4	2592.7	3024.5	3500.1	2561.3	2900.4	2865.6	2753.1	3205.7	2836.6	2027.7	3025.1	2494.6	2155.7	2664.7	3327.3	1572.4	1519.8	2426.0	733.8	2537.6
mn	15233.0	14631.0	6857.0	8885.6	9167.2	6127.1	7361.8	6620.2	6129.1	5957.3	7537.5	7363.9	7378.0	7614.9	7453.7	5847.4	6483.2	8322.4	9316.8	9835.1	11340.1	7743.7	5158.6	6800.7	2295.6	5738.8
la	2.07	1.15	21.02	9.56	0.99	5.07	4.04	4.87	3.34	6.79	0.20	1.82	0.06	0.46	0.11	6.39	0.91	1.31	3.30	2.90	8.86	0.08	52.63	0.06	62.12	30.60
ce	8.87	4.69	55.08	30.18	3.65	24.21	15.77	19.58	12.53	19.12	0.84	4.91	0.21	1.63	0.47	14.58	3.43	4.89	10.37	10.39	22.20	0.32	110.24	0.14	131.75	77.35
pr	1.96	1.08	7.79	4.77	0.49	4.01	2.90	3.44	2.28	2.83	0.20	0.68	0.03	0.26	0.08	1.88	0.55	0.73	1.39	1.58	3.02	0.08	12.87	0.03	16.87	11.29
nd	12.87	8.34	37.01	23.79	2.94	20.53	0.12	17.02	12.17	13.71	1.46	3.18	0.20	1.62	0.52	7.26	2.85	3.69	6.27	7.00	11.72	0.93	46.55	0.12	67.41	49.76
sm	4.94	3.48	11.11	7.00	1.26	7.49	6.48	6.38	4.27	4.98	1.08	1.21	0.09	0.60	0.21	1.47	1.48	1.59	2.07	2.71	3.37	0.97	8.70	0.06	13.71	12.82
eu	3.24	2.20	4.49	3.96	0.78	2.55	3.45	3.26	2.52	2.40	0.72	0.63	0.07	0.38	0.09	0.77	0.83	0.92	1.10	1.29	1.86	0.77	4.07	0.05	6.38	6.09
gd	9.41	4.79	12.94	9.68	2.54	7.10	6.88	6.90	5.24	5.43	1.32	1.28	0.32	0.58	0.28	1.19	1.67	1.71	2.68	2.42	2.75	1.67	11.09	0.09	17.59	14.27
gd	7.11	5.02	9.82	7.99	1.15	6.22	7.51	6.66	3.23	5.23	0.80	0.72	0.10	0.33	0.09	0.63	1.49	1.42	2.46	2.09	3.50	1.99	7.20	0.08	12.71	8.89
dy	4.49	3.19	8.32	6.46	0.66	4.32	6.33	5.48	3.03	3.78	0.91	0.59	0.10	0.30	0.06	0.67	1.40	1.51	1.98	1.98	2.81	1.21	5.05	0.13	10.87	8.05
er	1.54	1.61	2.66	1.45	0.20	0.71	1.49	1.32	0.51	0.99	0.04	0.19	0.07	0.10	0.06	0.24	0.42	0.43	0.60	0.53	0.79	0.37	1.23	0.05	3.51	2.09
yb	0.09	0.66	1.46	0.66	BDL	BDL	1.14	1.20	0.05	1.00	0.21	BDL	BDL	0.06	0.11	0.29	0.63	0.54	0.26	0.37	0.77	0.11	1.18	0.10	2.94	1.66
mn/fe	3.2	3.5	3.3	2.3	2.6	4.1	2.8	2.2	1.8	2.3	2.6	2.6	2.7	2.4	2.6	2.9	2.1	3.3	4.3	3.7	3.4	4.9	3.4	2.8	3.1	2.3
Ree (total)	56.6	36.2	171.7	105.5	14.7	82.2	56.1	76.1	49.1	66.3	7.8	15.2	1.3	6.3	2.1	35.4	15.7	18.7	32.5	33.3	61.7	8.5	260.8	0.9	345.9	222.9

S15272-*	4	5	6	7	3	8	9	10	11	12	13	14	15	16	17	18	19	22	23	2	1	20	21	24
fe	2780.4	4590.2	4427.0	4259.0	4430.4	4507.9	5454.2	4562.0	4857.0	5507.5	6070.5	6064.8	6372.4	5443.8	4440.3	83.0	4846.0	4189.0	4215.1	3637.7	3943.5	4027.6	2836.8	3537.8
mn	13958.8	11419.8	10044.8	9520.9	9629.0	9850.5	11242.8	9779.5	10538.8	11478.8	12198.8	10740.8	10722.8	15232.8	14027.8	3253.4	15757.8	12912.8	13897.8	11271.8	11907.8	12741.8	8044.3	11387.8
la	5.57	5.09	5.77	7.42	8.45	6.34	0.59	5.34	0.86	1.06	1.43	1.23	1.90	1.36	11.81	8.72	2.39	0.16	0.01	0.56	0.46	0.01	BDL	0.05
ce	16.77	14.93	16.45	20.51	20.17	16.97	2.14	14.32	2.14	2.88	2.65	4.75	4.91	3.48	14.49	41.76	2.92	0.67	0.42	1.35	1.38	0.61	41.67	30.24
pr	2.81	2.53	2.45	2.91	3.24	2.66	0.25	2.53	0.31	0.32	0.44	0.80	0.61	0.47	2.26	6.06	0.33	BDL	BDL	0.12	0.23	0.05	7.48	5.03
nd	15.50	11.71	13.04	15.19	15.68	10.57	1.53	10.49	0.35	3.56	1.25	3.48	5.22	1.89	11.98	28.70	2.30	1.70	0.25	BDL	0.90	0.03	37.98	26.54
sm	6.31	4.96	6.86	6.04	7.50	6.28	1.06	5.28	0.69	0.75	2.78	1.67	2.18	1.18	5.70	10.17	1.08	BDL	BDL	0.36	0.22	0.15	19.63	13.00
eu	1.50	1.50	1.48	1.65	1.95	1.28	0.21	1.28	0.10	0.11	0.10	0.19	0.39	0.34	1.30	4.28	0.17	0.18	BDL	0.16	0.15	0.04	4.73	3.12
gd	10.19	8.74	11.52	12.32	10.99	9.14	1.65	7.48	2.08	1.38	1.43	6.40	3.30	3.86	6.91	13.84	1.81	1.45	2.66	2.73	1.47	0.38	33.82	19.41
gd	8.61	7.29	8.45	8.45	9.86	9.51	2.48	7.08	0.99	1.31	1.52	3.59	4.44	2.58	9.97	10.40	2.17	0.93	1.12	1.29	1.91	0.23	29.06	21.25
dy	5.59	4.10	3.93	5.37	4.86	3.48	2.03	3.59	0.87	2.08	0.80	2.35	4.19	1.52	5.89	10.73	1.96	1.05	1.17	2.11	2.00	1.01	18.04	11.25
er	1.19	0.77	0.64	0.57	1.01	0.25	BDL	0.33	0.36	BDL	2.46	BDL	BDL	0.62	1.36	5.41	0.06	1.57	BDL	BDL	0.39	BDL	3.24	1.50
yb	0.46	0.64	1.09	1.19	0.57	0.91	BDL	0.18	0.12	BDL	1.30	BDL	BDL	0.17	1.17	5.06	0.13	BDL	0.64	BDL	0.41	0.14	3.18	2.94
mn/fe	5.0	2.5	2.3	2.2	2.2	2.2	2.1	2.1	2.2	2.1	2.0	1.8	1.7	2.8	3.2	39.2	3.3	3.1	3.3	3.1	3.0	3.2	2.8	3.2
REE(total)	74.5	62.3	71.7	81.6	84.3	67.4	11.9	57.9	8.9	13.4	16.2	24.5	27.1	17.5	72.8	145.1	15.3	7.7	6.3	8.7	9.5	2.7	198.8	134.3

Table 3

REE geochemical analyses of the Borrowdale Volcanic Group in Borehole 2, undertaken by ICP-MS. Fm/Mbr abbreviations are for rock units within the entire drilled BVG (Degnan et al 2003), from the top down: FIHi = Fleming Hall Formation; BBa = Brown Bank Formation; SeHa = Seascale Hall member of Brown Bank Formation; Blw = Bleawith Formation; BrFa = Broom Farm Formation; MoFa = Moor Farm Formation.

Fm/Mbr	Samp no.	DepthOD (m)	La	Ce	Pr	Nd	Sm	Eu	Gd	Dy	Ho	Er	Yb	Lu
FIHi	A303	-408.55	37.63	82.15	9.31	34.97	7.40	1.77	7.00	6.89	1.23	3.49	3.32	0.48
FIHi	A272	-425.53	38.57	85.04	9.57	35.56	7.68	1.85	7.11	7.14	1.28	3.63	3.46	0.49
FIHi	A270	-445.27	33.17	78.45	8.95	33.67	7.30	1.60	6.62	6.51	1.17	3.42	3.38	0.48
FIHi	A246	-454.68	38.03	82.98	9.54	35.77	7.63	1.84	7.21	7.12	1.27	3.58	3.42	0.49
FIHi	A238	-470.95	38.73	84.10	9.65	36.77	7.65	1.83	7.14	7.27	1.29	3.68	3.47	0.50
FIHi	A294	-487.77	39.07	88.69	9.94	36.98	7.99	1.93	7.53	7.56	1.35	3.86	3.67	0.52
FIHi	A259	-503.53	37.15	82.47	9.45	35.12	7.67	1.83	7.21	6.89	1.24	3.60	3.46	0.41
FIHi	A293	-534.11	35.64	80.95	9.15	34.09	7.46	1.75	7.17	7.15	1.28	3.63	3.46	0.50
FIHi	A298	-553.28	37.71	85.53	9.68	35.73	7.73	1.84	7.25	7.30	1.30	3.71	3.56	0.50
FIHi	A248	-569.42	36.96	83.53	9.20	34.33	7.01	1.68	6.41	6.46	1.16	3.30	3.13	0.45
FIHi	A262	-598.70	34.83	80.40	9.19	34.20	7.60	1.86	7.34	7.15	1.30	3.67	3.47	0.51
FIHi	A301	-628.21	35.56	82.13	9.28	34.75	7.56	1.87	7.14	7.13	1.27	3.61	3.43	0.49
FIHi	A304	-638.70	38.30	84.58	9.48	35.92	7.60	1.86	7.15	7.09	1.26	3.59	3.39	0.49
FIHi	A280	-646.60	36.35	82.04	9.27	34.54	7.57	1.87	7.11	7.08	1.27	3.58	3.41	0.49
FIHi	A290	-668.33	34.50	80.10	9.01	33.82	7.34	1.80	6.99	7.10	1.28	3.62	3.43	0.49
FIHi	A241	-691.20	37.16	82.80	9.61	36.12	7.72	1.82	7.14	7.14	1.27	3.61	3.42	0.49
FIHi	A287	-726.12	30.03	73.07	8.63	33.01	7.30	1.71	6.61	6.25	1.11	3.19	3.15	0.45
FIHi	A273	-745.20	25.56	60.31	7.02	25.25	5.55	1.18	5.31	6.02	1.12	3.26	3.17	0.45
FIHi	A267	-762.76	34.87	79.14	8.86	33.17	7.34	1.76	6.98	6.73	1.21	3.43	3.26	0.48
FIHi	A263	-787.01	35.14	79.45	8.90	32.99	7.33	1.77	7.03	6.69	1.12	3.40	3.22	0.47
BBa	A297	-825.34	28.64	71.65	8.10	30.52	6.68	1.41	6.28	6.01	1.06	2.98	2.80	0.40
BBa	A253	-853.50	28.40	66.33	7.94	30.23	6.35	1.38	5.63	4.97	0.88	2.49	2.40	0.35
SeHa	A277	-885.13	46.74	101.47	11.06	40.11	8.53	1.81	7.56	8.03	1.45	4.12	3.92	0.55
SeHa	A245	-902.57	47.46	102.92	11.11	40.93	8.39	1.84	7.29	7.75	1.42	4.17	4.08	0.58
SeHa	A260	-926.15	42.76	93.78	10.24	36.96	7.89	1.72	7.17	7.24	1.32	3.78	3.71	0.54
SeHa	A325	-960.95	48.13	103.41	11.28	41.07	8.48	1.85	7.87	7.93	1.41	4.03	3.92	0.56
SeHa	A324	-971.09	46.42	101.06	11.01	39.86	8.26	1.77	7.41	7.55	1.35	3.88	3.78	0.54
SeHa	A446	-989.29	46.12	101.13	11.04	39.46	8.43	1.81	7.78	8.20	1.48	4.14	3.95	0.57
BBa (tuff)	A445	-998.57	42.09	92.59	10.30	36.11	7.66	1.63	6.82	6.99	1.26	3.59	3.48	0.49
Blw	A428	-1027.95	42.09	91.28	10.18	36.61	7.95	1.84	7.21	7.15	1.28	3.70	3.55	0.51
Blw	A426	-1042.58	39.34	85.31	9.45	34.99	7.56	1.81	7.07	7.11	1.27	3.56	3.36	0.48
Blw	A431	-1081.98	38.13	83.70	9.41	34.97	7.61	1.84	7.03	6.91	1.24	3.49	3.30	0.48
Blw	A433	-1090.15	36.82	81.53	9.11	33.86	7.36	1.80	6.95	6.75	1.20	3.38	3.20	0.46
Blw	A441	-1116.67	38.88	85.79	9.72	34.68	7.59	1.76	6.98	6.93	1.25	3.52	3.36	0.48
Blw	A440	-1135.02	36.52	81.90	9.40	34.16	7.43	1.80	6.88	6.82	1.21	3.42	3.24	0.47
Blw	A438	-1145.89	34.62	77.30	8.74	32.46	6.95	1.73	6.51	6.47	1.15	3.24	3.08	0.44
Blw	A451	-1156.63	36.23	80.15	9.12	33.54	7.22	1.75	6.76	6.63	1.20	3.34	3.17	0.46
Blw	A452	-1181.97	35.28	78.13	8.87	32.69	7.08	1.81	6.71	6.63	1.19	3.34	3.09	0.45
Blw	A376	-1200.38	33.80	75.49	8.60	32.73	7.03	1.80	6.67	6.59	1.18	3.32	3.11	0.44
Blw	A408	-1233.72	36.25	82.15	9.25	34.43	7.39	1.83	6.89	6.84	1.22	3.45	3.23	0.46
Blw	A411	-1259.35	35.54	82.64	9.40	34.69	7.46	1.77	6.99	6.82	1.23	3.48	3.32	0.47
Blw	A413	-1278.45	38.03	84.70	9.47	35.17	7.62	1.89	7.15	7.08	1.27	3.59	3.39	0.48
Blw	A404	-1300.96	39.80	89.15	10.04	36.93	7.89	1.83	7.31	7.34	1.30	3.73	3.55	0.50
Blw	A418	-1326.55	39.34	86.88	9.55	35.09	7.61	1.81	7.10	7.01	1.26	3.57	3.42	0.49
Blw	A420	-1334.84	45.42	98.37	10.82	38.96	8.38	1.86	7.64	7.50	1.35	3.86	3.78	0.54
Blw	A385	-1362.02	43.23	94.18	10.44	37.38	7.85	1.67	6.99	7.13	1.31	3.77	3.64	0.52
Blw	A382	-1375.27	40.73	88.12	9.70	34.37	7.25	1.62	6.46	6.35	1.16	3.32	3.21	0.47
Blw	A421	-1394.77	32.59	73.53	8.17	29.40	6.53	1.45	6.31	6.96	1.28	3.74	3.53	0.50
Blw	A391	-1410.63	48.44	108.41	11.89	41.89	8.90	1.80	7.83	7.94	1.42	4.04	3.87	0.54
BrFa	A387	-1426.41	31.23	67.82	7.64	28.28	6.23	1.47	5.78	5.67	1.04	2.95	2.90	0.42
BrFa	A402	-1452.23	20.94	49.44	5.82	22.60	5.23	1.34	5.02	4.58	0.83	2.35	2.15	0.30
MoFa	A400	-1467.09	31.86	72.06	8.25	31.95	6.98	1.53	6.54	6.13	1.11	3.11	2.93	0.42
MoFa	A398	-1493.71	39.67	86.14	9.65	34.47	7.36	1.57	6.56	6.32	1.15	3.27	3.11	0.45
MoFa	A395	-1529.83	53.82	118.50	13.14	46.77	9.81	1.40	8.78	9.14	1.62	4.59	4.38	0.61
MoFa	A399	-1541.03	54.93	120.64	13.18	46.18	9.79	1.12	8.87	9.64	1.75	5.08	5.03	0.70

Figure 1. Location of boreholes on a simplified geological map of Sellafield, UK.

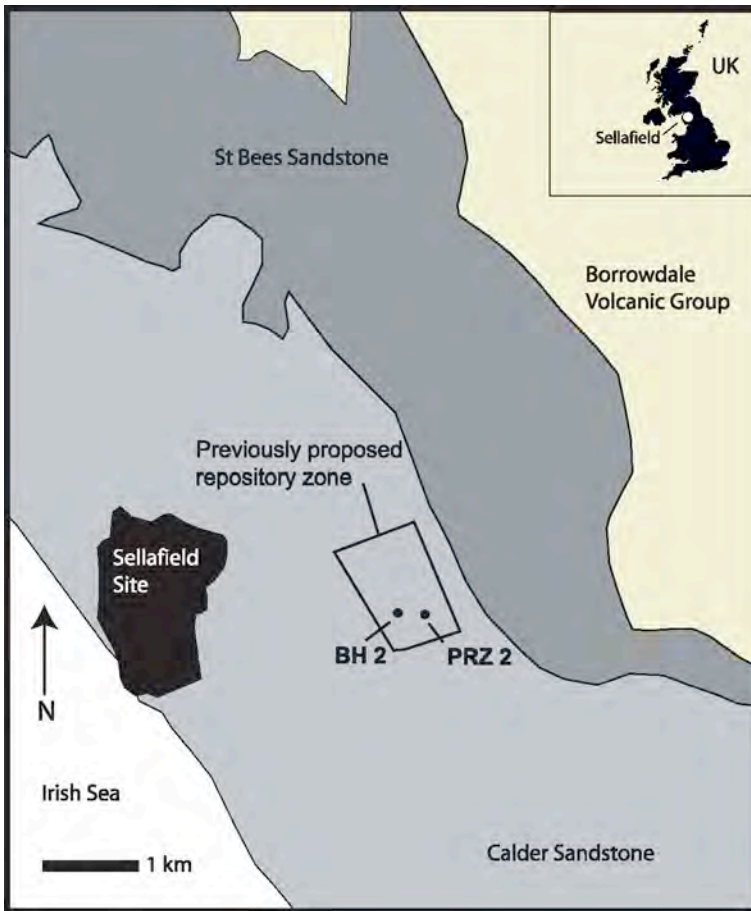


Figure 2. Young (ME9) calcite fracture-fill morphology from the Sellafield subsurface. Scanning Electron Microscope Secondary Electron (SEM-SE) images depict calcite with (A) ‘nailhead’ morphology and (B) ‘dogtooth’ morphology. The depth profile (C) combines data from adjacent boreholes BH2 and PRZ 2 within the ‘Proposed Repository Zone, illustrating the distribution of morphological types of late calcite compared to present day groundwater salinity (modified after Milodowski et al., 1998).

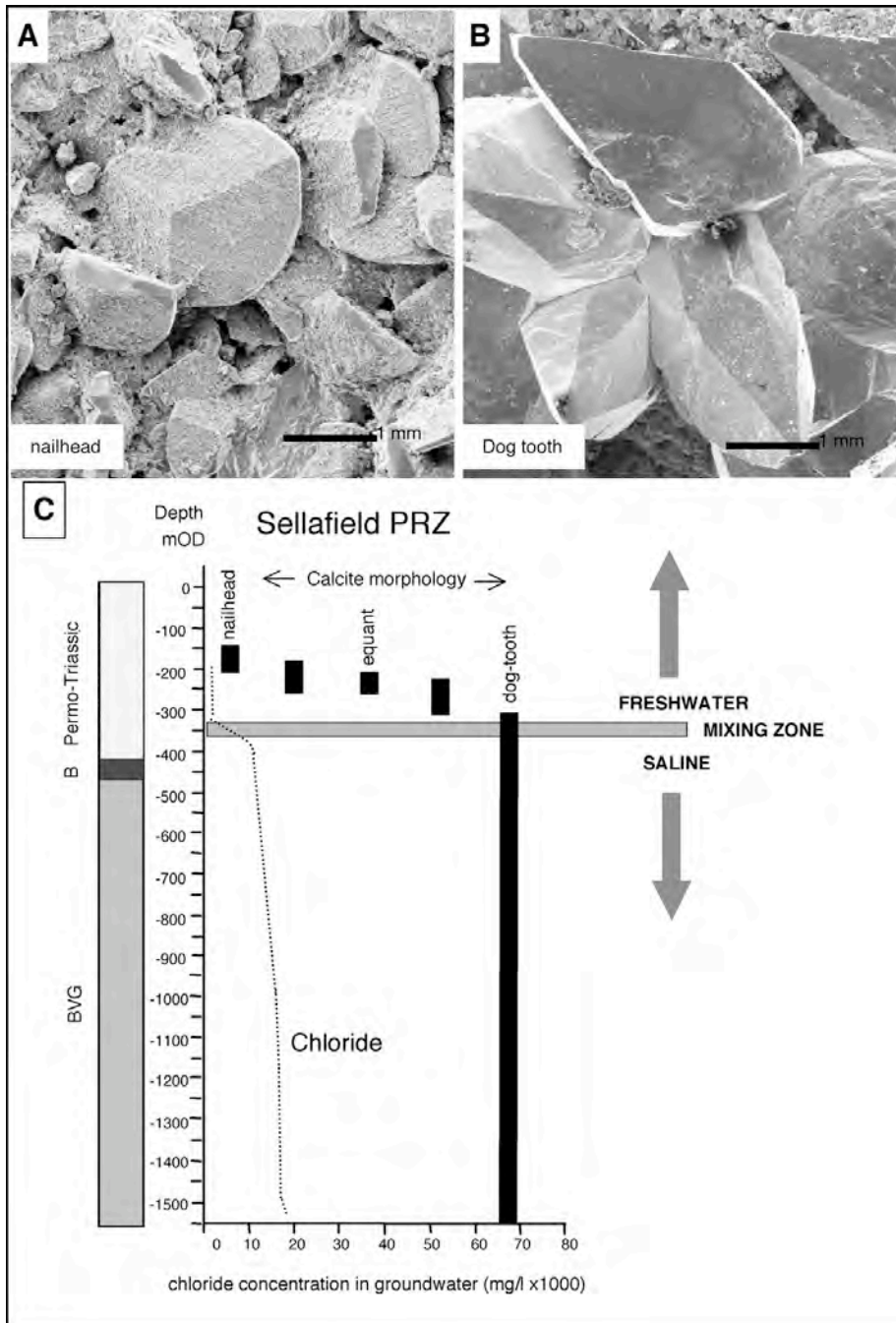


Figure 3. Calcite ME9 fracture-fill calcite at Sellafield shows a general increase in both Fe and Mn concentrations (ppm) with depth. This is due to a general (though not uniform) decrease of redox with depth. Symbols depict sample depth in metres.

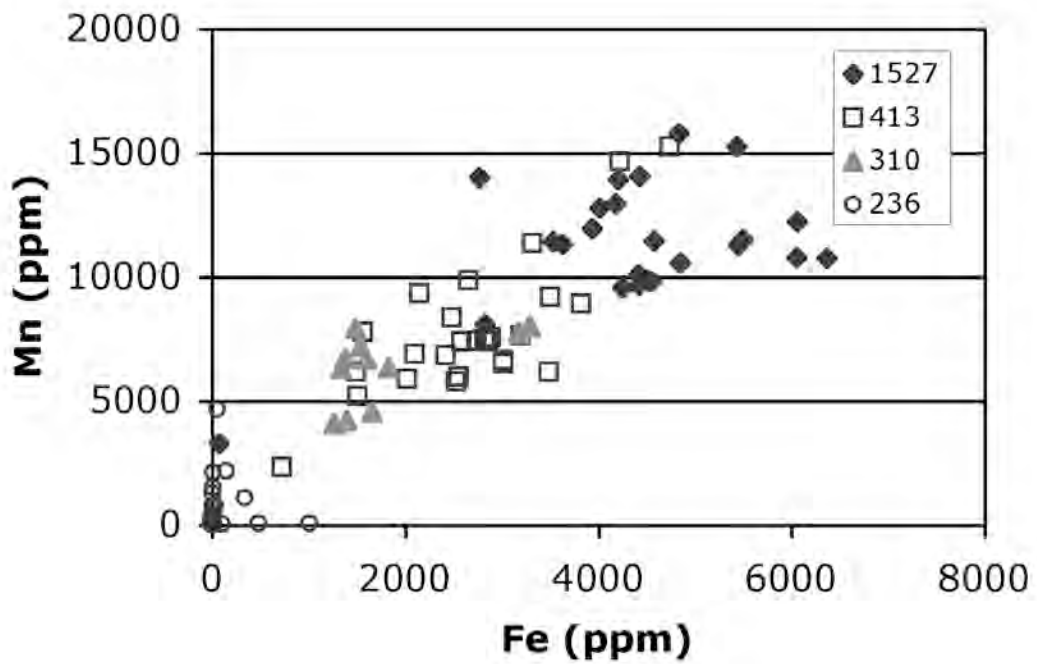


Figure 4. Mn to Fe ratios along an ion microprobe traverse of ME9 fracture-fill calcite crystals sampled from 236m and 1527m b.o.d. at Sellafield. Mn:Fe appear relatively stable in the deeper sample, due to stable redox conditions. By contrast the ratio fluctuates greatly in the shallower calcite, due to varying redox.

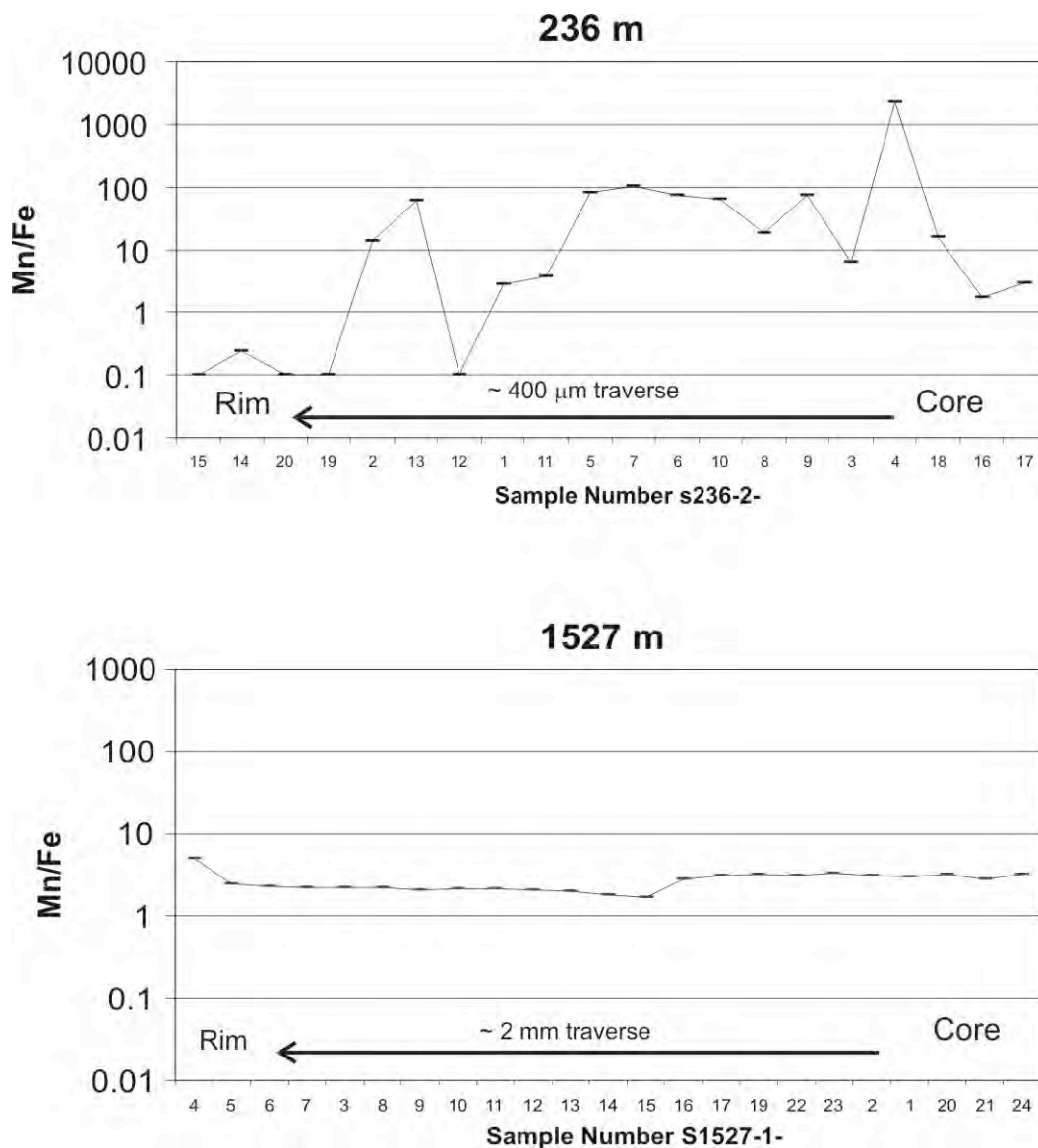


Figure 5. Combined CL images and Chondrite-normalised REE patterns of late fracture-fill calcite at Sellafield. Calcites have been sampled from: (A) 236m, (B) 310m, (C) 413m, and (D) 1527m. Analytical spot locations are coloured dots on CL images. For simplification, analyses with similar Chondrite-normalised REE profiles have been grouped as dots of similar colour within each individual crystal. Note that this portrays a fluctuation of REE conditions through successive CL zones, changing to-and-from states of local recurrent equilibrium. See text for details. Data derived from Table 2.

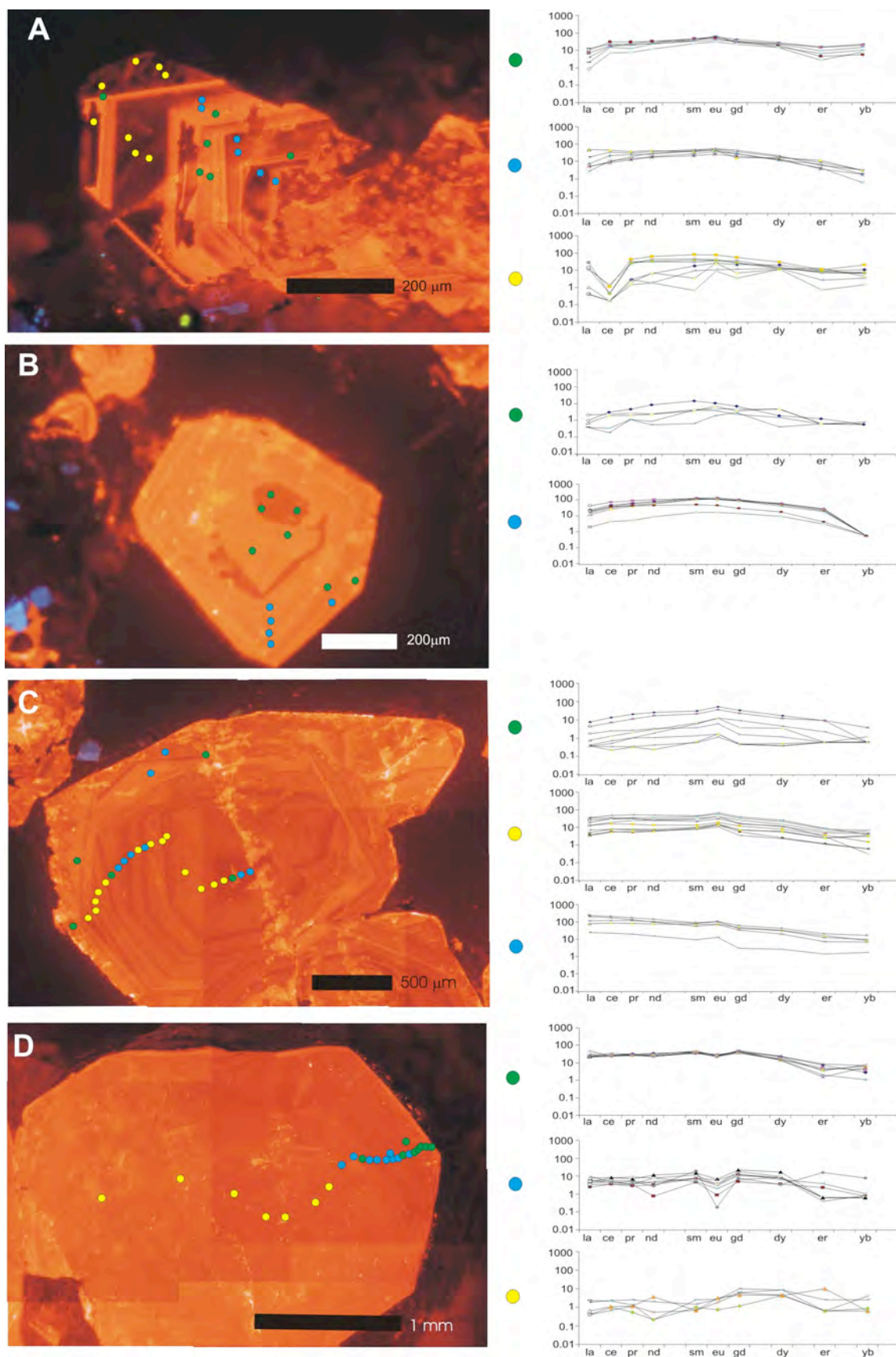


Figure 6. Chondrite-normalised REE patterns from whole rock sampled across the Borrowdale Volcanic Group in BH2 (see Table 3). Overall, all the BVG variants demonstrate a similar profile, with systematically less HREE, and depletion in Eu.

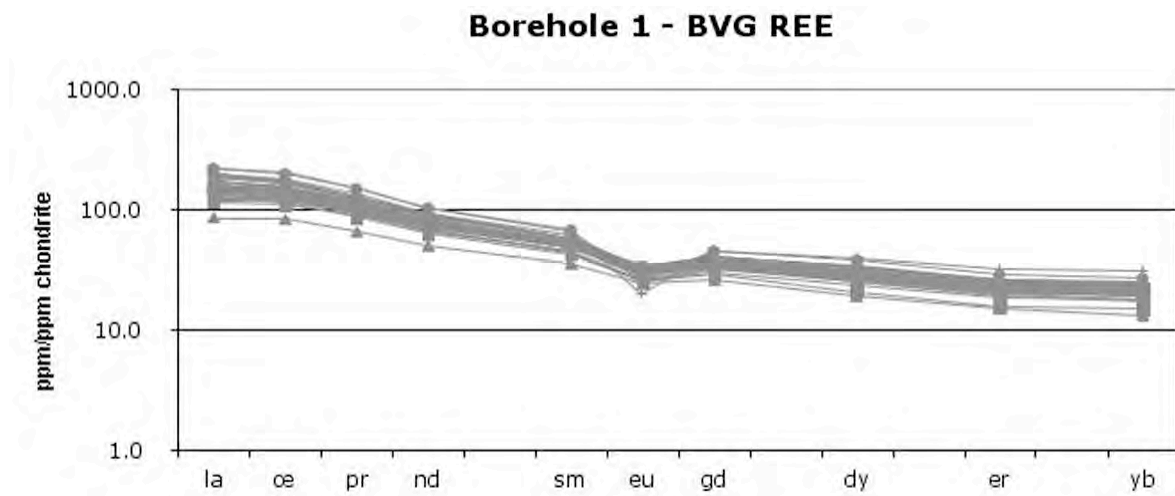


Figure 7. REE plots of St Bees Sandstone at Sellafield. Analyses from whole-rock core samples by conventional ICP methods. A weak Eu depletion is apparent, however no Ce anomaly is detected, so that the REE anomaly in calcites at 236m is not due to host-rock effects.

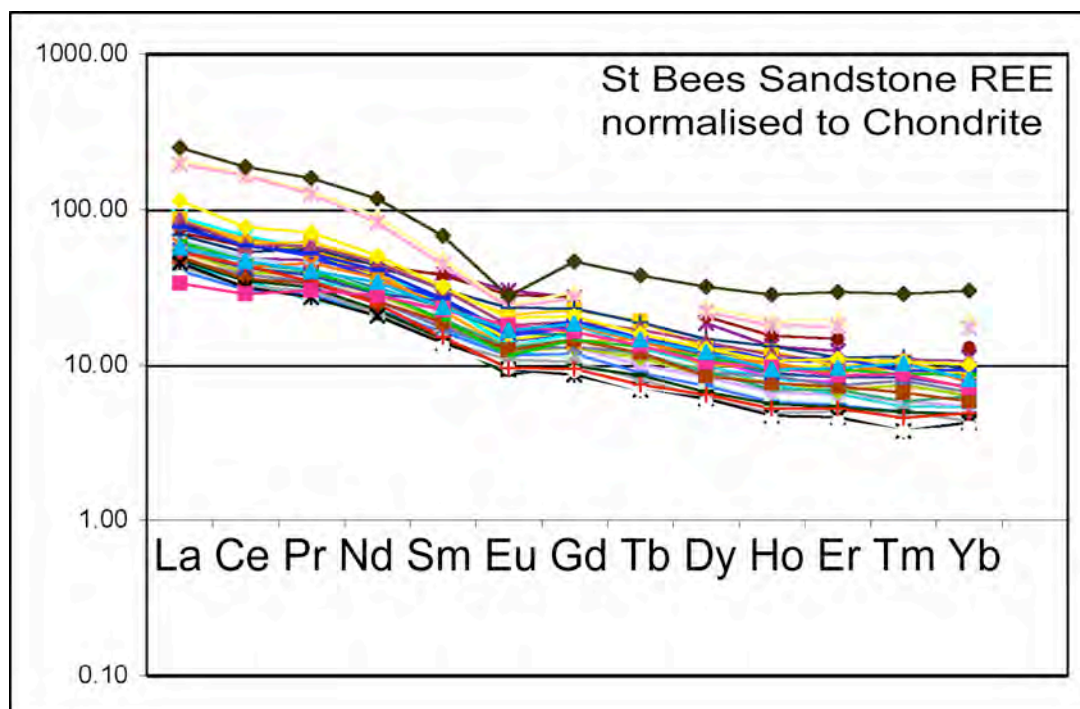


Figure 8

Stability field diagram redrawn from Brookins 1989, showing that the stability of Eu^{3+} is reduced to Eu^{2+} only in conditions more reducing than -0.35 volts or over the pH range of about 6 to 9. Therefore in this palaeo-aquifer, the stable state will be Eu^{3+} because redox conditions never reached as negative as -350mV .

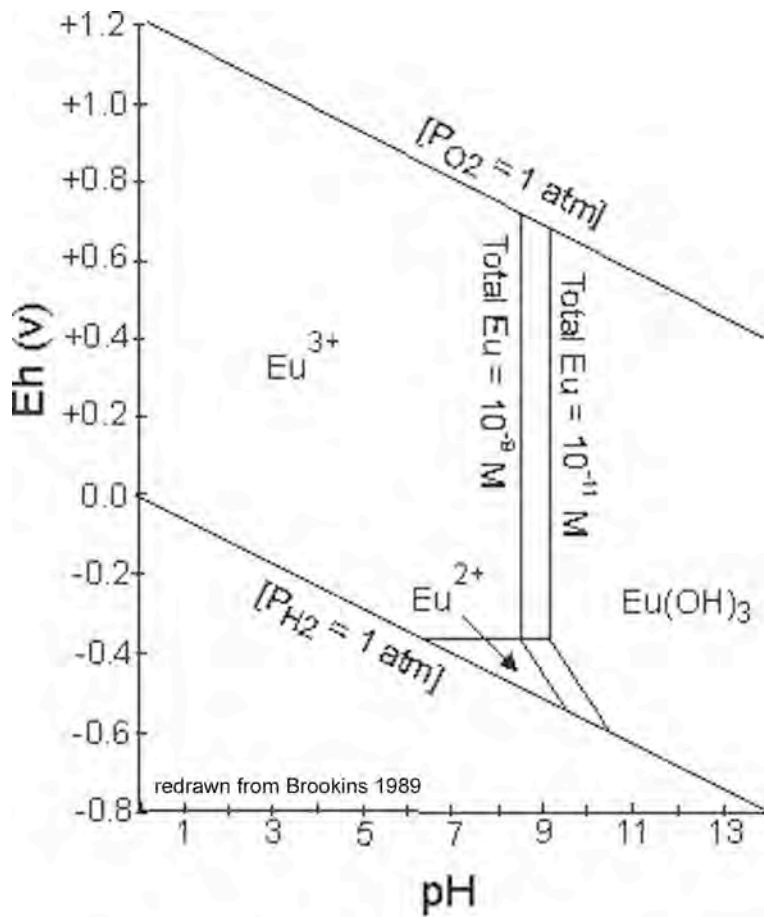


Figure 9

Stability field diagram, redrawn from Brookins 1989, showing that Ce is reduced at a range of Eh conditions, dependent on the Ce concentration, and on the pH. The deep groundwaters at present day Sellafield, have pH of 7.8 to 6.2. Horizontal arrows for mid-range pH of 7.0, show the Ce redox boundary lies between +40 and +160mV, but could be as reduced as -150 mV in more alkaline groundwater. Thus if pH was 7.0, Ce in Sellafield shallow 236m groundwater was usually reduced at an Eh of less than +50mV, but unusual conditions enabled periodic oxidation to +160mV. Such conditions were plausibly due to influx of oxidised sub-glacial water.

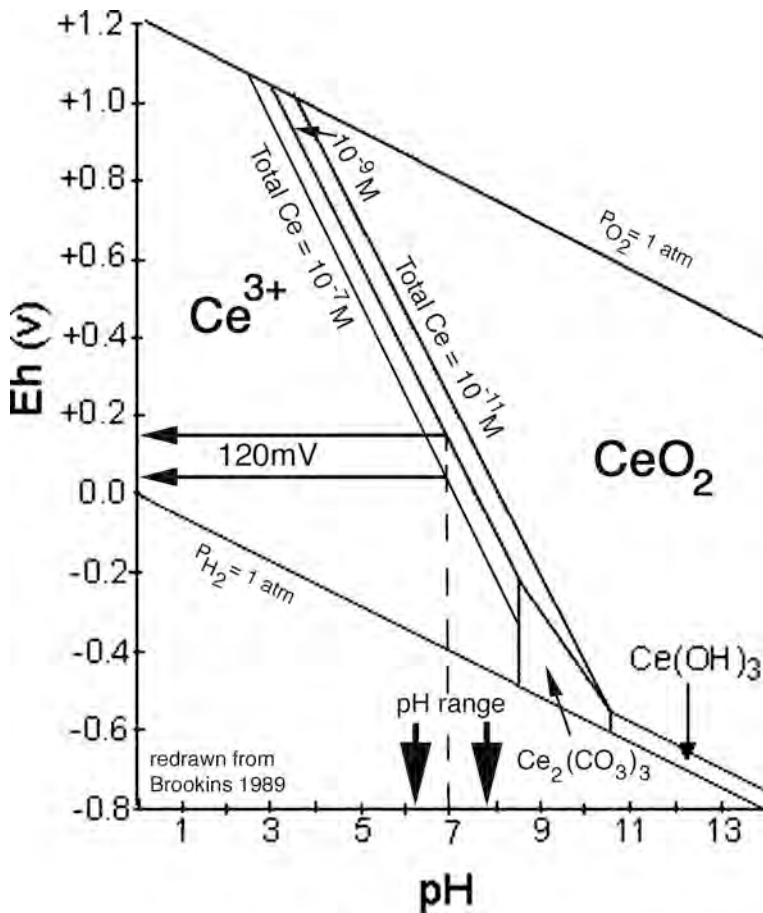


Figure 10. Cross-section SW-NE through BH2, redrawn from Haszeldine (1996), with additional data for the lower limit of mineralization ME8 from Milodowski (unpub), which shows the depth at which any visible traces of sulphide mineralization exist co-genetic with, or post-dating, ME9 calcites. Data on sulphides taken from core logs in Nirex reports. A systematic pattern exists, of shallow Fe-Mn (hydr)oxides, overlying deeper sulphides. We interpret this to be an indication of redox, with relatively more reduced mineral assemblages occurring deeper.

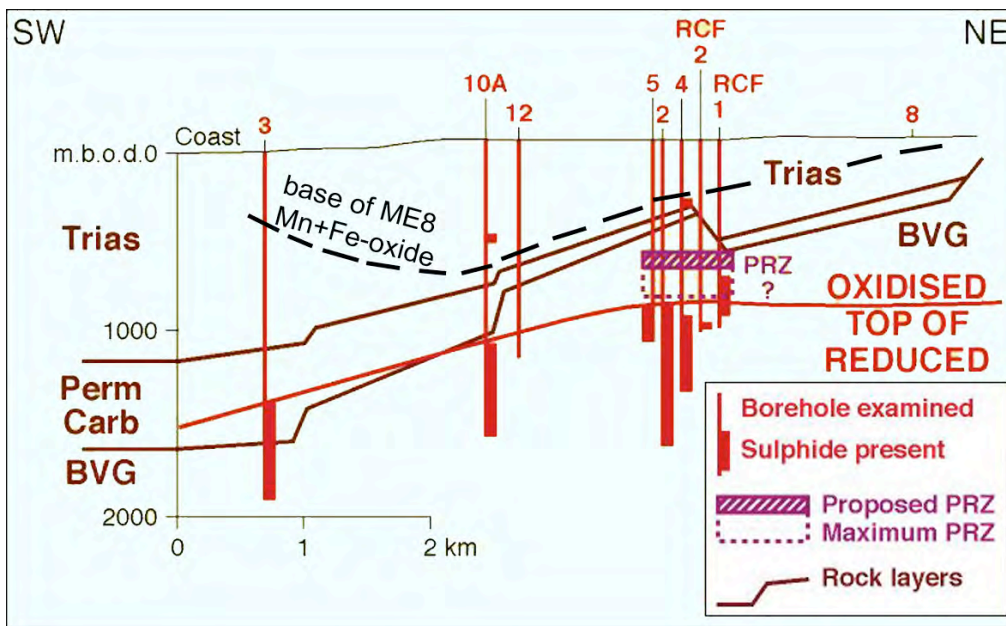


Figure 11. Speculative summary of interpreted redox depth through the Quaternary deposition of ME9 calcites at Sellafield. Time-scale can not, as yet, be refined.

